Int. J. Heat Mass Transfer. Vol. 33, No. 8, pp. 1675–1683, 1990
Printed in Great Britain

0017-9310/90 $3.00 + 0.00

Forced convection of thermally developing laminar flow in circular sector ducts

Q. M. LEI and A. C. TRUPP
Department of Mechanical Engineering, University of Manitoba, Winnipeg, Manitoba, Canada R3T 2N2

(*Received* 24 *May* 1989 *and in final form* 10 *October* 1989)

Abstract—Numerical solutions are presented for laminar, forced convection heat transfer in the thermal entrance region of circular sector ducts using the H1 and H2 thermal boundary conditions. With fully developed hydrodynamics, results are given for duct apex angles of 20°, 45°, 90°, 130°, 180°, 270°, and 360°. For the H1 condition, decreasing apex angle increases the duct corner effects, hence enhancing local and fully developed Nusselt numbers and shortening thermal entrance sections. For the H2 condition, the apex angle influences the thermal quantities differently. The data presented are compared with the limited available solutions and good agreement is found.

INTRODUCTION

ANALYSES OF forced convection heat transfer in circular sector ducts are often encountered in engineering applications, e.g. for flow through a multi-passage tube. Also, such analysis provides a lower bound for the problem of combined free and forced convection which has received much attention in recent years. Primarily, the present investigation was motivated by our experimental study of buoyancy effects on forced convection in a horizontal semicircular duct [1, 2]. Since one practical heating means is heating by electric resistance wires (like our experimental set-up), this analysis considers the boundary condition of axially uniform heat flux. The peripheral conditions employed are uniform wall temperature and uniform wall heat flux, denoted by H1 and H2, respectively.

Previous theoretical investigations for circular sector ducts have been mainly limited to laminar fluid flow and forced convection in the fully developed region. Some of these characteristics have been compiled by Shah and London [3]. Lei and Trupp [4–6] have recently extended this work and provided the fully developed pressure drop data and Nusselt numbers over the entire apex angle range for a number of thermal boundary conditions. For the problem of hydrodynamically fully developed and thermally developing flow, Manglik and Bergles [7] numerically predicted Nusselt numbers for an isothermal semicircular tube. Regarding the H1 condition, only one investigation for a semicircular tube was reported by Hong and Bergles [8]. When studying internally fined tubes, Prakash and Liu [9] reported local Nusselt numbers for three circular sector ducts, but for the flow of simultaneous development of velocities and temperature. This theoretical study involves the developing temperature with the fully developed hydrodynamics which corresponds to the behavior of fluids with high Prandtl numbers. Results presented in this paper for the H1 and H2 conditions over the whole apex angle range of circular sector ducts are also useful for designing compact heat exchangers.

ANALYTICAL FORMULATION

Figure 1 shows the duct cross-section under consideration. The analysis is limited to the steady, laminar flow of incompressible Newtonian fluids with constant properties. The fluid axial heat conduction is considered to be negligible. For circular tubes at least, this idealization is valid [3], except for the immediate neighborhood of the duct inlet, providing $(Re\ Pr) > 50$. Like most laminar flow analyses, this study also neglects viscous dissipation within the fluid. Using dimensionless variables and parameters defined in the Nomenclature, the governing differential equations can be written as follows:

momentum equation

$$\frac{\partial^2 w}{\partial r^2} + \frac{1}{r}\frac{\partial w}{\partial r} + \frac{1}{r^2}\frac{\partial^2 w}{\partial \theta^2} = C \tag{1}$$

energy equation

$$\frac{\partial^2 T}{\partial r^2} + \frac{1}{r}\frac{\partial T}{\partial r} + \frac{1}{r^2}\frac{\partial^2 T}{\partial \theta^2} = w\left(\frac{\partial T}{\partial x} + A\right). \tag{2}$$

The boundary conditions for equation (1) are

$$w(r,0) = w(1,\theta) = 0, \quad \text{and} \quad \frac{\partial w}{\partial \theta}(r,\phi) = 0 \tag{3}$$

where the last condition corresponds to the symmetry line defined by $\theta = \phi$. Equation (2) is supplemented by the following boundary conditions:

at $x = 0$

$$T = 0 \quad \text{for all } r \text{ and } \theta \tag{4}$$

at $x > 0$

for the H1 condition

NOMENCLATURE

A	geometry parameter, $2(\phi+1)/\phi$
C	dimensionless pressure drop parameter, $(R_0^2/\mu\bar{W})(\partial P/\partial X)$
c_p	specific heat
D_h	hydraulic diameter, $2\phi R_0/(\phi+1)$
H1	axially uniform wall heat flux with uniform peripheral wall temperature
H2	axially and peripherally uniform heat flux
$\bar{h}$	peripherally averaged heat transfer coefficient, equation (9)
k	fluid thermal conductivity
L_T, L_T^0	thermal entrance length, $L_T = X_T/(D_h Re_h Pr)$ and $L_T^0 = X_T/(R_0 Re_0 Pr)$
Nu, Nu_0	peripherally averaged Nusselt number, equations (10) and (12)
n	normal coordinate
P	pressure
Pr	Prandtl number, $\mu c_p/k$
q''	peripherally averaged wall heat flux at each section
R, r	radial coordinate, $r = R/R_0$
R_0	radius of the duct
Re_h, Re_0	Reynolds number, $Re_h = \rho D_h \bar{W}/\mu$ and $Re_0 = \rho R_0 \bar{W}/\mu$
T, t	temperature, $T = (t-t_m)/(q'' R_0/k)$
$\bar{T}_w, \bar{t}_w$	average wall temperature at any section, $\bar{T}_w = (\bar{t}_w - t_m)/(q'' R_0/k)$
T	constant wall temperature both peripherally and axially
W, w	axial velocity, $w = W/\bar{W}$
$\bar{W}$	cross-sectional mean axial velocity
X, x	axial coordinate, $x = X/(R_0 Re_0 Pr)$.

Greek symbols

δ_f	fluid mean conduction path length
θ	angular coordinate
μ	fluid dynamic viscosity
ρ	fluid density
ϕ	half apex angle of the circular sector duct.

Subscripts

fd	fully developed conditions
H1	for the H1 boundary condition
H2	for the H2 boundary condition
m	bulk mean
T	thermal entrance length or the T boundary condition
w	at duct wall
x	axially local.

$$T = T_w \quad \text{at } r = 1, \quad 0 \leqslant \theta \leqslant \phi$$
$$\text{and at } \theta = 0, \quad 0 \leqslant r < 1 \tag{5a}$$

(note that T_w is a function of x)

$$\frac{\partial T}{\partial \theta} = 0 \quad \text{at } \theta = \phi, \quad 0 < r < 1; \tag{5b}$$

for the H2 condition

$$\frac{\partial T}{\partial r} = 1 \quad \text{at } r = 1, \quad 0 \leqslant \theta \leqslant \phi \tag{6a}$$

$$\frac{\partial T}{\partial \theta} = -r \quad \text{at } \theta = 0, \quad 0 \leqslant r < 1 \tag{6b}$$

$$\frac{\partial T}{\partial \theta} = 0 \quad \text{at } \theta = \phi, \quad 0 < r < 1. \tag{6c}$$

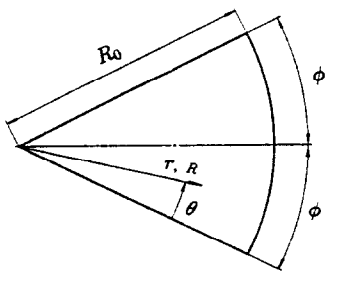

FIG. 1. Cross-section of the circular sector duct.

It is noted that the wall temperatures (T_w) at each cross-section are not known in advance for both the cases. To solve for T, a solution method is first to use equation (4) at the duct inlet. Then the solution procedure is progressed along the axial direction. At each axial station, wall temperatures must be initially guessed while equation (2), together with its boundary conditions, is solved for the T distribution. Wall temperatures are then corrected by determining the dimensionless bulk mean temperature. After several iterations, the correct velocity and local temperature fields must ensure that

$$T_m = \frac{2}{\phi}\int_0^{\phi}\int_0^1 Twr\,dr\,d\theta = 0. \tag{7}$$

As the solution step is marched, the temperature profile gradually develops. In a far downstream region, $\partial T/\partial x$ approaches zero and the temperature field becomes independent of the axial coordinate. Consequently, in such a fully developed region, equation (2) reduces to

$$\frac{\partial^2 T}{\partial r^2} + \frac{1}{r}\frac{\partial T}{\partial r} + \frac{1}{r^2}\frac{\partial^2 T}{\partial \theta^2} = Aw. \tag{8}$$

Complete series solutions for this equation with both the H1 and H2 boundary conditions have been provided previously. The accurate fully developed Nusselt numbers reported in refs. [5, 6] were used in this

study in connection with grid size selection as discussed later. The cross-sectional-average heat transfer coefficient, $\bar{h}$, is defined in customary manner as

$$q'' = \bar{h}(\bar{t}_w - t_m). \tag{9}$$

Using the dimensionless peripheral average wall temperature $\bar{T}_w$ and the hydraulic diameter D_h, the Nusselt number is given by

$$Nu = \frac{\bar{h}D_h}{k} = \left(\frac{2\phi}{\phi+1}\right)\frac{1}{\bar{T}_w} \tag{10}$$

where $\bar{T}_w = T_w$ for the H1 condition, but for the H2 condition, $\bar{T}_w$ can be evaluated by

$$\bar{T}_w = \frac{1}{\phi+1}\left(\int_0^1 T(r,0)\,dr + \int_0^\phi T(1,\theta)\,d\theta\right). \tag{11}$$

Since D_h is a function of the duct apex angle, to better isolate the ϕ effect and to facilitate comparison to a circular tube, the Nusselt number may be defined, on the basis of duct radius R_0, as

$$Nu_0 = \frac{\bar{h}R_0}{k} = \frac{1}{\bar{T}_w}. \tag{12}$$

Information on the thermal entrance length is also of practical importance. Thus, in this analysis, values of thermal entrance lengths were taken as the dimensionless distances where the local Nusselt numbers first drop to within 1.05 and 1.01 times the fully developed Nusselt numbers, denoted by L_{T5}^0 and L_{T1}^0, respectively. Similarly, the conventional thermal entrance length, L_T, was correspondingly defined with the axial distance normalized by $(D_h\,Re_h\,Pr)$. The relationship between L_T and L_T^0 for circular sector ducts is given by†

$$L_T = \left(\frac{\phi+1}{2\phi}\right)^2 L_T^0. \tag{13}$$

COMPUTATIONAL PROCEDURE

The finite difference equation (2) was formulated using control volume integration. For the velocity field, the exact solution to equation (1) with equation (3) was computed from the series expression in ref. [4]. At a given axial station, equation (2) with equation (5) or equation (6) was numerically solved by a band storage linear equation solver. Iterations were needed for obtaining the correct T distribution. Thus, a number of corrections (2–5 for most stations) were made on the wall temperature for the H1 condition and on an arbitrary nodal temperature for the H2 condition, while ensuring that the bulk mean temperature was less than 10^{-6} in magnitude. For each case, the solution procedure was marched along x until the local Nusselt number was at least within 0.1% of the corresponding fully developed value as numerically generated from equation (8).

Decisions on the adequacy of the cross-sectional mesh size adopted for each duct geometry were mainly guided by comparing a numerical value of $(Nu)_{fd}$ to the exact value obtained from the series solution [5, 6]. Table 1 gives these comparisons and the mesh sizes used in this investigation. For both the cases, the chosen mesh sizes were taken to be fine enough to make a grid value of $(Nu)_{fd}$ within 0.5% of the exact solution value. Regarding the axial step size, the marching step size Δx for the study was also determined by numerical experimentation. For example, for $2\phi = 180°$, with the cross-sectional mesh size (22×25) fixed and the first step size $\Delta x = 10^{-6}$, two numerical tests were conducted near the entrance. One let Δx be increased by 5% and another by 25% for each consecutive station. Local Nusselt numbers from these two tests showed no noticeable difference. This insensitivity to the axial step size is mainly attributed to the use of the accurate direct solver for simultaneous linear equations at each cross-section. For all cases, it was finally decided to use the following pattern. The first step size was taken as $\Delta x = 10^{-6}$. Then Δx was increased by 20% for each subsequent step size. Upon reaching 8×10^{-4}, Δx remained unchanged for the rest of the entrance section. Using these three-dimensional meshes, specific tests were run which positively confirmed that the three-dimensional temperature profile for each case was indeed converging to the two-dimensional fully developed temperature profile for the same cross-sectional grid.

RESULTS AND DISCUSSION

The following section provides information on the thermal entrance region of seven circular sector ducts. For the largest apex angle ($2\phi = 360°$), the results correspond to a circular tube with one internal full fin.

Fully developed results

Nusselt numbers for hydrodynamically and thermally fully developed flow were generated by solving equation (8) numerically. These results, together with values determined from series solutions [5, 6], are given in Table 1. For both the H1 and H2 conditions, all present Nusselt numbers fell within 0.5% of the exact solution values with an average difference of about 0.1%. This excellent agreement can be seen (for Nu_0 only) in Fig. 2, which shows variations of fully developed Nusselt numbers with duct apex angle. Both Nusselt numbers (Nu based on D_h and Nu_0 based on R_0) have been plotted, but as can be seen, $(Nu)_{fd}$ tends to mask the ϕ effect. For instance, $(Nu_{H1})_{fd}$ decreases with decreasing ϕ which is accompanied by increasing corner effects. In fact, for the H1 condition, this increase of corner effects should enhance the duct capability of thermal energy transfer. The reason for

† Inasmuch as one of the objectives in this study is to examine the ϕ effect, the use of these two pairs of definitions for Nu and L_T is useful.

Table 1. Mesh size and fully developed results

2ϕ (deg)	$r \times \theta$	$(Nu_{H1})_{fd}$ Present	$(Nu_{H1})_{fd}$ Exact [5]	$(Nu_{H2})_{fd}$ Present	$(Nu_{H2})_{fd}$ Exact [6]
20	22 × 15	2.7683	2.7633	0.3692	0.3710
45	22 × 17	3.2820	3.2792	1.7592	1.7630
90	22 × 20	3.7460	3.7440	2.9871	2.9870
130	22 × 22	3.9485	3.9466	3.0282	3.0280
180	22 × 25	4.0897	4.0880	2.9210	2.9200
270	30 × 35	4.2113	4.2178		
	22 × 30			2.7704	2.7690
360	50 × 40	4.2653	4.2852		
	22 × 32			2.6876	2.6870

this is as follows: since $\bar{h}_{H1} = -k(\overline{\partial t/\partial n})/(t_w - t_m)$, where t_w is constant, introducing the fluid mean effective conduction path length δ_f (as in ref. [3]) yields $\bar{h}_{H1} = k(t_w - t_m)/\delta_f/(t_w - t_m) = k/\delta_f$. Accordingly, a circular sector duct with smaller ϕ should have a shorter overall δ_f value, and this means a higher average heat transfer coefficient. Concerning the H2 condition, a parallel analysis suggests that wall temperatures at corners are higher than temperatures for surfaces away from the corners. Hence since $\bar{h}_{H2}$ involves the evaluation of average wall temperature, the ϕ effect on $\bar{h}_{H2}$ should not be as marked as on $\bar{h}_{H1}$. On the other hand, as is shown in Fig. 2, Nu_0 follows the expected trends of heat transfer coefficients versus apex angle for both cases. Note that a maximum for $(Nu_{0,H2})_{fd}$ occurs at $2\phi \approx 60°$. This particular circular sector duct has an $(Nu_{0,H2})_{fd}$ value which falls between the Nusselt values for equilateral triangular ducts with two rounded corners and no rounded corners [3].

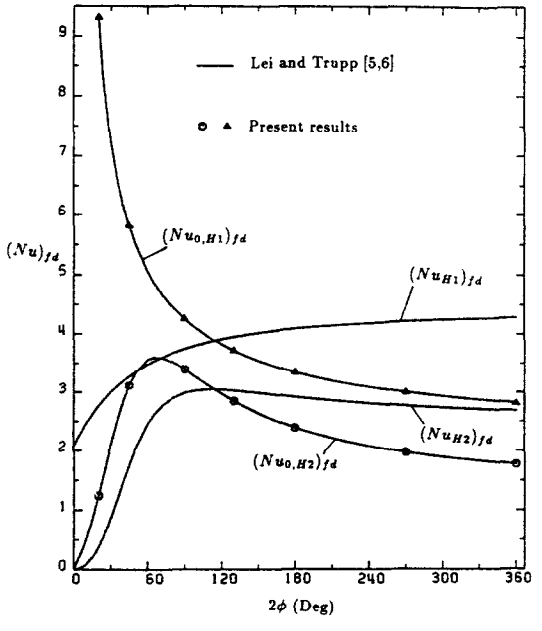

FIG. 2. Fully developed Nusselt numbers for circular sector ducts.

Thermally developing flow heat transfer

Results for $Nu_{x,H1}$ and $Nu_{x,H2}$ in the thermal entrance region for the seven circular sector ducts are presented in Table 2. For convenience, the dimensionless axial distance x is normalized by the corresponding thermal entrance length L^0_{T1} as previously defined (values for L^0_{T1} will be tabulated later). It should be noted that Table 2 can also be used to estimate the flow length average Nusselt number which is often required in a heat exchanger design.

Local Nusselt numbers for the H1 *condition.* Figure 3 shows the variations of the local H1 Nusselt numbers for four of the circular sector ducts. As indicated before, the hydraulic diameter D_h is intentionally removed from the plot to better disclose the apex angle effect. For each circular sector duct, $Nu_{0x,H1}$ exhibits the expected trend of a monotonic decrease with x, approaching the limiting value of $(Nu_{0,H1})_{fd}$ in the fully developed region. Except for very near the duct inlet ($x < 8 \times 10^{-5}$), local values for $Nu_{0x,H1}$ demonstrate the same ϕ variation as the $(Nu_{0,H1})_{fd}$ values, namely an increase with decreasing apex angle.

For comparison purposes, Fig. 3 also includes the results of other investigators for other ducts. As can be seen in Fig. 3, all non-circular ducts including the one internal full-fin tube ($2\phi = 360°$) possess higher Nusselt numbers than a circular tube, except for very close to the duct inlet. For a semicircular tube ($2\phi = 180°$), the present $Nu_{0x,H1}$ values compare well in Fig. 3 with the results of Hong and Bergles [3, 8]. Differences between the local Nusselt numbers averaged 2.7%, but were always within 7%. Figure 3 also shows a comparison with two non-circular ducts whose Nusselt numbers fall between the curves of circular sector ducts with $2\phi = 45°$ and 90°. These two ducts are the equilateral triangular duct (comparable with the circular sector duct of $2\phi = 60°$) and the right-angled isosceles triangular duct (comparable with the circular sector duct of $2\phi = 90°$). Using the same basis of R_0 (see Fig. 3 for R_0 definition), the $Nu_{0x,H1}$ values for these two ducts appear to have correct trends with x as well as with ϕ. For instance, higher values of $Nu_{0x,H1}$ for the right-angled isosceles triangular duct are definitely expected when compared to the values for the circular sector duct of $2\phi = 90°$.

Table 2. Variation of Nusselt numbers in the entrance region of circular sector ducts

	$2\phi = 20°$		$2\phi = 45°$		$2\phi = 90°$		$2\phi = 130°$		$2\phi = 180°$		$2\phi = 270°$		$2\phi = 360°$	
x/L_{T1}^0	$Nu_{x,H1}$	$Nu_{x,H2}$	$Nu_{x,H1}$	$Nu_{x,H2}$	$Nu_{x,H1}$	$Nu_{x,H2}$	$Nu_{x,H1}$	$Nu_{x,H2}$	$Nu_{x,H1}$	$Nu_{x,H2}$	$Nu_{x,H1}$	$Nu_{x,H2}$	$Nu_{x,H1}$	$Nu_{x,H2}$
0.0001	37.852	9.268	40.809	28.988	44.494	49.603	46.674	51.663	48.602	51.923	58.871	49.247	60.794	45.641
0.0005	22.653	4.812	27.270	17.214	31.850	32.231	34.084	32.330	35.454	30.605	36.330	26.664	34.856	23.739
0.0010	17.880	3.583	22.203	13.308	26.497	25.198	28.141	24.606	28.907	22.881	28.161	19.850	27.429	17.870
0.0030	12.349	2.236	15.888	8.706	18.756	16.392	19.409	15.655	19.545	14.585	19.004	12.930	18.758	11.795
0.0050	10.461	1.796	13.542	7.124	15.682	13.363	16.138	12.791	16.216	12.024	15.909	10.715	15.747	9.807
0.0070	9.386	1.559	12.133	6.243	13.915	11.732	14.302	11.264	14.379	10.626	14.185	9.506	14.061	8.697
0.0100	8.385	1.343	10.763	5.441	12.251	10.242	12.609	9.882	12.700	9.344	12.579	8.382	12.487	7.663
0.0200	6.733	1.013	8.472	4.210	9.629	7.949	9.946	7.731	10.046	7.320	10.011	6.577	9.960	6.043
0.0300	5.916	0.864	7.379	3.641	8.405	6.891	8.700	6.721	8.802	6.368	8.774	5.738	8.739	5.292
0.0400	5.404	0.775	6.709	3.306	7.651	6.246	7.922	6.096	8.024	5.781	8.011	5.227	7.984	4.835
0.0500	5.040	0.713	6.233	3.069	7.129	5.800	7.384	5.662	7.480	5.377	7.474	4.873	7.456	4.520
0.0700	4.547	0.633	5.614	2.754	6.418	5.189	6.648	5.085	6.746	4.839	6.759	4.405	6.752	4.105
0.1000	4.099	0.563	5.050	2.475	5.764	4.639	5.981	4.565	6.081	4.356	6.115	3.986	6.121	3.737
0.1500	3.680	0.499	4.509	2.223	5.143	4.120	5.350	4.080	5.457	3.906	5.511	3.599	5.529	3.402
0.2000	3.436	0.463	4.189	2.084	4.778	3.818	4.981	3.799	5.093	3.646	5.162	3.377	5.189	3.212
0.2500	3.281	0.441	3.975	1.998	4.537	3.619	4.737	3.616	4.854	3.475	4.934	3.233	4.968	3.090
0.3000	3.169	0.425	3.824	1.940	4.365	3.479	4.565	3.487	4.686	3.356	4.775	3.133	4.814	3.006
0.4000	3.024	0.405	3.627	1.871	4.141	3.297	4.341	3.321	4.470	3.200	4.572	3.004	4.618	2.898
0.5000	2.937	0.393	3.508	1.834	4.005	3.190	4.207	3.222	4.342	3.107	4.452	2.927	4.502	2.832
0.6000	2.883	0.385	3.433	1.812	3.920	3.122	4.123	3.160	4.261	3.047	4.376	2.879	4.428	2.789
0.7000	2.848	0.380	3.384	1.798	3.863	3.079	4.067	3.118	4.208	3.007	4.326	2.846	4.380	2.760
0.8000	2.824	0.377	3.352	1.789	3.826	3.050	4.030	3.091	4.172	2.981	4.293	2.824	4.347	2.740
0.9000	2.807	0.375	3.330	1.782	3.801	3.030	4.005	3.072	4.148	2.963	4.270	2.809	4.323	2.725
1.0000	2.796	0.373	3.315	1.777	3.783	3.017	3.988	3.058	4.131	2.950	4.253	2.798	4.308	2.715
1.2000	2.782	0.371	3.298	1.770	3.764	3.002	3.968	3.043	4.110	2.935	4.234	2.785	4.288	2.702
1.5000	2.774	0.370	3.287	1.765	3.752	2.992	3.955	3.033	4.097	2.926	4.220	2.776	4.275	2.693

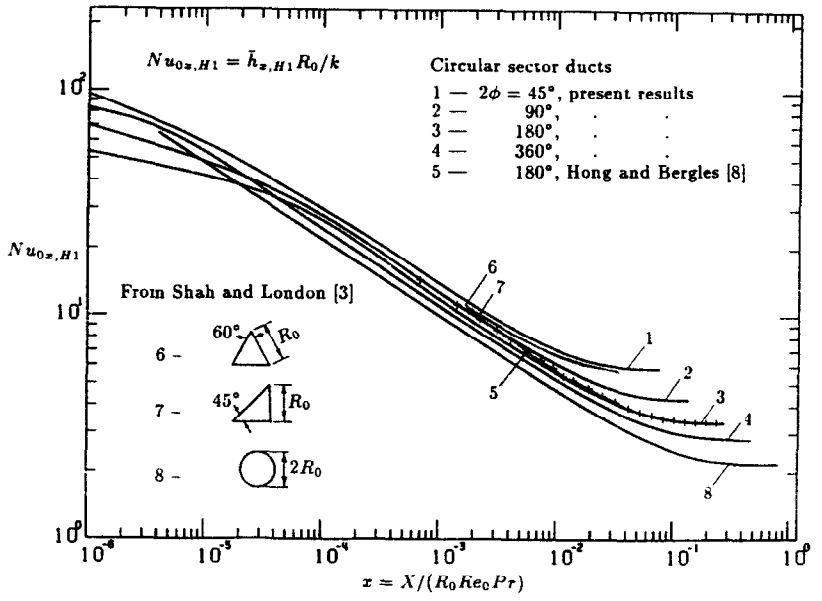

FIG. 3. Comparison of $Nu_{0x,H1}$ with other published results.

As demonstrated before, this is because the fluid mean effective conduction path length for the right-angled isosceles triangular duct is relatively shorter.

Local Nusselt numbers for the H2 *condition.* Variations of $Nu_{0x,H2}$ for the thermally developing flow for the seven circular sector ducts plus a square duct are graphically shown in Fig. 4. Like $Nu_{0x,H1}$, for each duct, $Nu_{0x,H2}$ monotonically drops as x increases. In the far downstream region, each curve approaches its correct fully developed value of $(Nu_{0x,H2})_{fd}$. It should also be pointed out that, near the entrance, Fig. 4 appears to show flatter slopes for $Nu_{0x,H2}$ than for further downstream. This misleading appearance is due to the logarithmic scale plotting. The actual slopes of Nu_{0x} versus axial distance for all cases of this study were always steepest near the entrance.

Concerning the ϕ effect, for $x \geq 6 \times 10^{-2}$, local values of $Nu_{0x,H2}$ for all circular sector ducts in Fig. 4 follow the same pattern as $(Nu_{0,H2})_{fd}$ versus ϕ, as displayed in Fig. 2, i.e. increasing the apex angle up to 60° gives rise to an increase in $Nu_{0x,H2}$ which then decreases with further increases in ϕ. For the middle region of the flow development, the ϕ effect on $Nu_{0x,H2}$ is very small for $2\phi > 45°$. Figure 4 also provides one

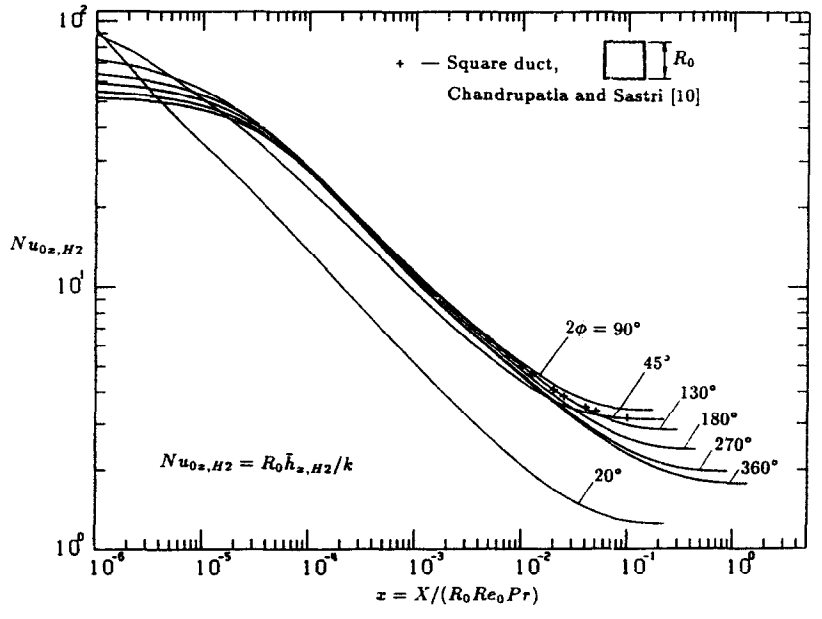

FIG. 4. Local Nusselt numbers for the H2 condition.

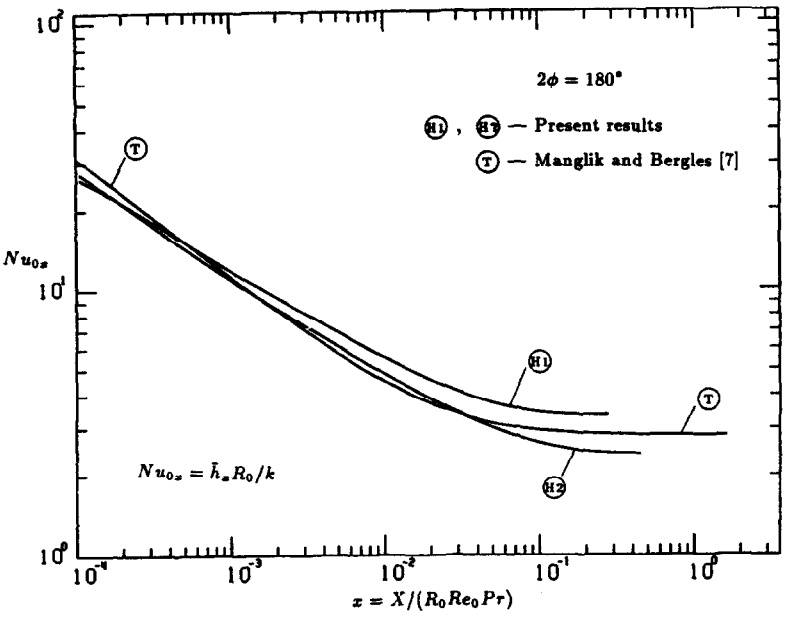

FIG. 5. Local Nusselt numbers for a semicircular duct with different boundary conditions.

comparison to the $Nu_{0x,H2}$ results of Chandrupatla and Sastri [10], who studied non-Newtonian fluids in a square duct. Their Newtonian results of $Nu_{0x,H2}$ appear between the curves of the circular sector ducts for $2\phi = 90°$ and 130°. This would also be the case if their Newtonian results of $Nu_{0x,H1}$ were plotted in Fig. 3 (not plotted because of crowding).

Effect of thermal boundary conditions on Nu_{0x}. The differences between Nusselt numbers for the different thermal boundary conditions are considered next for each geometry. All results obtained in this investigation indicated that, except for the region very near the duct inlet, $Nu_{0x,H1}$ was always higher than $Nu_{0x,H2}$. This expected outcome is shown graphically in Fig. 5 using the semicircular tube as a typical example. It can be seen that, near the duct inlet, $Nu_{0x,H1}$ starts to exceed $Nu_{0x,H2}$. As the flow continues to develop, the difference between them increases and reaches up to about 40% (i.e. $(Nu_{0,H1})_{fd}/(Nu_{0,H2})_{fd} \approx 1.4$) in the fully developed region. Figure 5 also shows the developing Nusselt numbers for constant wall temperature in both the axial and peripheral directions (T) which were calculated from the correlation equation of the axial length mean Nusselt number (after conversion to $Nu_{0x,T}$) reported by Manglik and Bergles [7]. As illustrated, the $Nu_{0x,T}$ values fall between the curves of $Nu_{0x,H1}$ and $Nu_{0x,H2}$ as the flow approaches the fully developed region.

Thermal entrance length. Table 3 lists results of the thermal entrance lengths for the H1 and H2 conditions. For the semicircular tube ($2\phi = 180°$), the present values of 0.05395 and 0.09747 for $L_{T5,H1}$ and $L_{T1,H1}$ compare reasonably well with 0.0525 and 0.0893 respectively (obtained by interpolating the thermal entrance results of Hong and Bergles [3, 8] using the $(Nu_{H1})_{fd}$ value of 4.108 [8]). The differences are 3% for $L_{T5,H1}$ and 8% for $L_{T1,H1}$. For each geometry and boundary condition, Table 3 presents significantly higher values for L_{T1} than for L_{T5}. As a result, the $L_{T5,H1}$ entrance lengths average 56% of the $L_{T1,H1}$ values while results for $L_{T5,H2}$ average 54% of the $L_{T1,H2}$ values. These indicate (as expected) that the flow develops very gradually near the fully developed region. Furthermore, each $L_{T,H2}$ value listed in Table 3 is higher than its $L_{T,H1}$ counterpart. On average, the thermal entrance length for the H2 condition is 2.8 times longer than the section for the H1 condition. This indicates that the H1 condition, when imposed on a circular sector duct, is a much stronger thermal boundary condition (compared to H2) such that the temperature field requires a much shorter axial length for its full development. The thermal entrance results of Chandrupatla and Sastri [10] for a square duct also show that the H2 condition results in longer thermal entrance lengths than the H1 condition for Newtonian as well as non-Newtonian fluids.

For the H1 condition, a study of the data in Table 3 was made to determine the effect of apex angle on thermal entrance length. For $L_{T,H1}$, for large ϕ, thermal entrance lengths appear almost constant; however, for $2\phi \leqslant 100°$, $L_{T,H1}$ (which is normalized by D_h) increases with decreasing ϕ. In fact, physical variations of thermal entrance length are better viewed in terms of $L^0_{T,H1}$ (normalized by R_0), which show a monotonically increasing trend with ϕ. For small ϕ, duct corner effects assist early temperature development so that the trend is expected. Note that increasing the apex angle up to 360° (which forms a circular tube with one internal full fin) results in the largest thermal entrance length for each base, e.g. $L^0_{T5,H1} =$

Table 3. Results of thermal entrance length

	2ϕ						
	20°	45°	90°	130°	180°	270°	360°
$L^0_{T5,H1}$	0.01004	0.02345	0.04501	0.06203	0.08057	0.10657	0.12583
$L^0_{T1,H1}$	0.01822	0.04044	0.07749	0.10919	0.14556	0.19935	0.23870
$L^0_{T5,H2}$	0.07607	0.04524	0.05393	0.09367	0.14896	0.26030	0.39179
$L^0_{T1,H2}$	0.13466	0.09878	0.09377	0.16624	0.26542	0.48814	0.75257
$L_{T5,H1}$	0.11372	0.07373	0.05814	0.05489	0.05395	0.05406	0.05467
$L_{T1,H1}$	0.20631	0.12716	0.10011	0.09663	0.09747	0.10112	0.10371
$L_{T5,H2}$	0.86124	0.14225	0.06967	0.08290	0.09975	0.13203	0.17023
$L_{T1,H2}$	1.52464	0.31060	0.12114	0.14712	0.17773	0.24760	0.32698

0.12583. This value is still shorter than 0.17221 for a circular tube [3] which has no 'corner effects' at all.

For the H2 condition, again, $L^0_{T,H2}$ rather than $L_{T,H2}$ provides a better picture of the ϕ effect. Beyond $2\phi \gtrsim 45°$, corner effects diminish as the $L^0_{T,H2}$ values increase gradually with ϕ. It is noted that minima occur at $2\phi \approx 45°$ for $L^0_{T5,H2}$ and at $2\phi \approx 90°$ for $L^0_{T1,H2}$. Such behavior may be attributed to the $(Nu_{0,H2})_{fd}$ versus ϕ pattern which has a maximum value at $2\phi \approx 60°$, as shown in Fig. 2.

CONCLUDING REMARKS

In this study, numerical solutions were obtained for constant property, laminar fluid flow in the thermal entrance region of circular sector ducts. With the fully developed velocity field, the employed thermal boundary conditions H1 and H2 simulate non-circular ducts with high and low thermal conductivities in the peripheral direction, respectively. Results of forced convection heat transfer in the fully developed region agreed excellently with the existing data. Local Nusselt numbers for the semicircular tube with the H1 condition compared well with results in refs. [3, 8]. The data presented, which cover the entire apex angle range, were used to study the apex angle effects on heat transfer quantities of interest. It was observed that the apex angle influences these quantities differently for these two boundary conditions. Compared to H2, the H1 condition is thermally stronger, hence resulting in higher heat transfer coefficients and shorter thermal entrance lengths. However, in the absence of buoyancy effects, real situations would generally lie between the two, e.g. for a duct with an electric resistance wiring heating. On the other hand, for our experimental investigation of combined laminar convection in a horizontal semicircular duct, the present analytical results will serve as lower boundaries for the data.

Acknowledgement—This research was supported by the Natural Sciences and Engineering Research Council of Canada.

REFERENCES

1. Q. M. Lei and A. C. Trupp, Correlation of laminar mixed convection for a horizontal semicircular duct, *12th Can. Congr. Appl. Mech.*, pp. 704–705 (1989).
2. Q. M. Lei, Numerical and experimental study of laminar mixed convection in a horizontal semicircular duct, Ph.D. Thesis, University of Manitoba, Winnipeg, Canada (1990).
3. R. K. Shah and A. L. London, *Laminar Flow Forced Convection in Ducts*, Supplement 1 to *Advances in Heat Transfer*, Academic Press, New York (1978).
4. Q. M. Lei and A. C. Trupp, Maximum velocity location and pressure drop of fully developed laminar flow in circular sector ducts, *ASME J. Heat Transfer* **111**, 1085–1087 (1989).
5. Q. M. Lei and A. C. Trupp, Further analyses of laminar flow heat transfer in circular sector ducts, *ASME J. Heat Transfer* **111**, 1088–1090 (1989).
6. Q. M. Lei and A. C. Trupp, Laminar flow heat transfer in circular sector ducts with uniform heat flux, *Trans. Can. Soc. Mech. Engrs* **13**, 31–34 (1989).
7. R. M. Manglik and A. E. Bergles, Laminar flow heat transfer in a semicircular tube with uniform wall temperature, *Int. J. Heat Mass Transfer* **31**, 625–636 (1988).
8. S. W. Hong and A. E. Bergles, Laminar flow heat transfer in the entrance region of semicircular tubes with uniform heat flux, *Int. J. Heat Mass Transfer* **19**, 123–124 (1976).
9. C. Prakash and Ye-Di Liu, Analysis of laminar flow and heat transfer in the entrance region of an internally finned circular duct, *J. Heat Transfer* **107**, 84–91 (1985).
10. A. R. Chandrupatla and V. M. K. Sastri, Laminar forced convection heat transfer of a non-Newtonian fluid in a square duct, *Int. J. Heat Mass Transfer* **20**, 1315–1324 (1977).

CONVECTION FORCEE D'UN ECOULEMENT LAMINAIRE THERMIQUEMENT ETABLI DANS DES CONDUITES EN SECTEUR CIRCULAIRE

Résumé—Des solutions numériques sont présentées pour la convection thermique laminaire dans la région d'entrée des conduites en secteur circulaire avec les conditions aux limites thermiques H1 et H2. Pour des régimes hydrodynamiques établis, les résultats sont donnés pour des angles au centre de 20°, 45°, 90°, 130°, 180°, 270° et 360°. Pour la condition H1, une décroissance de l'angle augmente les effets de coin, provoquant l'accroissement des nombres de Nusselt locaux et raccourcissant les longueurs d'établissement thermique. Pour la condition H2, l'angle au centre influence différemment les caractéristiques thermiques. Les résultats présentés sont comparés aux solutions limitées disponibles et on trouve un bon accord.

ERZWUNGENE KONVEKTION IM THERMISCHEN EINLAUFGEBIET EINER LAMINAREN STRÖMUNG IN KREISSEKTOR-FÖRMIGEN KANÄLEN

Zusammenfassung—Die laminare erzwungene Konvektion im thermischen Einlaufgebiet von kreissektorförmigen Kanälen wird numerisch untersucht. Dabei werden als Randbedingungen konstante Wandtemperatur und konstante Wärmestromdichte verwendet. Für hydrodynamisch vollständig ausgebildete Strömung werden Ergebnisse für die folgenden Sektorwinkel angegeben: 20°; 45°; 90°; 130°; 180°; 270° und 360°. Bei konstanter Wandtemperatur steigt die Bedeutung der Winkeleffekte mit abnehmendem Sektorwinkel an, was zu einer Erhöhung der örtlichen und vollständig entwickelten Nusselt-Zahl führt. Das thermische Einlaufgebiet wird dadurch kleiner. Für aufgeprägte Wärmestromdichte ist der Einfluß des Sektorwinkels uneinheitlich. Die Ergebnisse werden mit den begrenzt vorhandenen Lösungen verglichen, die Übereinstimmung ist gut.

ВЫНУЖДЕННАЯ КОНВЕКЦИЯ ПРИ ТЕРМИЧЕСКИ РАЗВИВАЮЩЕМСЯ ЛАМИНАРНОМ ТЕЧЕНИИ В КРУГЛЫХ СЕКТОРАЛЬНЫХ КАНАЛАХ

Аннотация—Представлены результаты численного решения задачи о ламинарном конвективном теплопереносе в тепловом начальном участке каналов с сечением в форме кругового сектора при тепловых граничных условиях I и II рода. Приведены результаты для углов раскрытия сектора 20°, 45°, 90°, 130°, 180°, 270° и 360° в случае полностью развитой гидродинамики. При граничных условиях I рода с уменьшением раскрытия сектора влияние угла в канале усиливается, что приводит к увеличению локальных и установившихся чисел Нуссельта и к уменьшению начального участка. При граничных условиях II рода угол раскрытия сектора иначе влияет на тепловые величины. Полученные данные удовлетворительно согласуются с имеющимися немногочисленными решениями.